

Highly selective proton conductive networks based on chain-end functionalized polymers with perfluorosulfonate side groups†‡

Kui Xu, Chalathorn Chanthad, Michael A. Hickner and Qing Wang*

Received 5th January 2010, Accepted 3rd March 2010

DOI: 10.1039/c000044b

The copolymers of vinylidene fluoride and perfluoro(4-methyl-3,6-dioxane-7-ene) sulfonyl fluoride containing amino end-groups were synthesized for the first time. The prepared amino-terminated polymers underwent cross-linking reactions with 1,3,5-benzene trisocyanate to form proton conductive networks. The prepared membranes exhibited excellent thermal, hydrolytic and oxidative stabilities. The ion exchange capacity, water uptake, the state of absorbed water, and transport properties of the membranes were found to be highly dependent upon the chemical composition of the copolymers. The cross-linked membranes showed extremely low methanol permeability, while maintaining high proton conductivity at the same order of magnitude as Nafion. This unique transport feature gave rise to exceedingly higher electrochemical selectivity in relation to Nafion. The selectivity characteristics have been rationalized based on the formation of restrained ionic domains and the state of the absorbed water within the membranes.

Introduction

Fuel cells are considered one of the most promising energy conversion technologies by virtue of their relatively low-temperature operation, solid-state design, and their high efficiencies across a large range of sizes.¹ In particular, direct methanol fuel cells (DMFCs) have the potential to become high density power sources for portable and mobile applications such as microelectronics. Methanol has a volumetric energy density of 4800 Wh l⁻¹, which is an order of magnitude greater than state-of-the-art lithium batteries. If this energy can be harvested electrochemically in an efficient matter, DMFCs can drastically increase the run-time of many portable electronics applications and enable new power-hungry mobile devices. However, the use of liquid methanol as fuel causes other complications to the fuel cell system. A critical issue associated with this is methanol crossover,^{2,3} namely the tendency of methanol crossing from the anode, through the polymer electrolyte membrane (PEM), to the cathode catalytic layer. The presence of methanol at the cathode hampers oxygen reduction by occupying a part of the active catalyst sites and leads to a mixed potential that lowers cell voltage.⁴ Other concomitant negative impacts include severely reduced fuel utilization and aggravated water management issues.⁵ Nafion, the current state of the art PEM material, is known to have a poor barrier property to methanol permeation, and performs poorly in DMFCs.^{3,6}

Considerable efforts have thus been devoted to the exploration of new approaches to PEMs exhibiting a lower intrinsic methanol permeability than Nafion.⁷ These strategies include hydrocarbon electrolyte polymers,^{8–10} incorporation of inorganic additives into Nafion or other polymer matrix,^{11–13} and cross-linked polymers and blends.^{14–18} Nonetheless, in these alternative materials, a great depression in methanol permeation is accompanied by a severe decrease in proton conductivity. The trade-off between reduced methanol permeability and decreased conductivity leads to a marginal improvement in electrochemical selectivity, *i.e.* the ratio of proton conductivity over methanol permeability, which is a well accepted figure-of-merit to evaluate the potential of membrane performance in DMFCs. The relative electrochemical selectivity to Nafion for most PEMs with sufficient conductivity (*i.e.* > 0.01 S cm⁻¹) is less than 10.⁷

Here, we present the preparation and characterization of the chain-end cross-linked fluoropolymer networks showing extraordinarily high electrochemical selectivities. Cross-linking has been demonstrated as a promising approach to decreasing the methanol permeability *via* restricting the water adsorption of PEMs.¹⁴ Electron-beam and γ -irradiation have been applied to PEMs to induce cross-linking, which also results in chain scission and yields membranes with poor mechanical properties.¹⁹ Cross-linking reactions have been performed through a reaction with the sulfonic acid groups to form inter/intra-chain bridges.^{20,21} However, utilization of sulfonic acid groups leads to a decrease in ion content of the membranes, and consequently a lower proton conductivity. Another cross-linking approach involves incorporation of co-monomers with pendant functional moieties followed by a reaction with a multifunctional curing agent.²² Unfortunately, the resulting cross-linked structures are often difficult to control and undesirable degrees of cross-linking are obtained, which restricts proton diffusion rates in the membranes.

Different from the literature approaches, the present study is based on the functionalization of polymer chain ends and

Department of Materials Science and Engineering, The Pennsylvania State University, University Park, Pennsylvania, 16802, USA. E-mail: wang@matse.psu.edu; Fax: +1 814-865-2917; Tel: +1 814-863-0042

† This paper is part of a *Journal of Materials Chemistry* themed issue on proton transport for fuel cells. Guest editors: Sossina Haile and Peter Pintauro.

‡ Electronic supplementary information (ESI) available: Additional characterisation and humidity dependence data. See DOI: 10.1039/c000044b

subsequent utilization of functional end-groups in the cross-linked reaction to yield proton conductive networks. It is anticipated that the selective placement of cross-linkable groups at polymer chain ends can keep the main-chain structure of the fluoropolymer intact and thus preserve their unique physical properties such as excellent electrochemical stability and superior acidity. Moreover, the chain-end cross-linking approach would maintain continuity of the proton conduction channel of linear polymers to a great extent. By varying polymer molecular weights and the relative ratio between the polymer and curing agent, molecular structures and domain sizes of the cross-linked networks can be systematically tuned for optimized properties.

Experimental

1,3,5-Benzene triisocyanate was prepared according to the literature procedures.²³ Vinylidene fluoride (VDF) and perfluoro(4-methyl-3,6-dioxane-7-ene) sulfonyl fluoride (PFSVE) were purchased from SynQuest Laboratory Inc. and used as received. All other chemicals and solvents were purchased from VWR international, Inc. and used as received unless otherwise mentioned.

Synthesis

4,4'-tert-Butoxycarbonylamino benzoyl peroxide. To a mixture of DCC dichloromethane solution (5 mL, 1M) and H₂O₂ aqueous solution (5 mL, 30%), 4-butoxycarbonylamino benzoic acid (1.2 g, 5.1 mmol) in dichloromethane was added slowly at -10 °C. The reaction mixture was stirred at 0 °C for 6 h. The reaction mixture was filtered and the filter cake was washed with cold dichloromethane several times. The filtrates were combined and the solvent was evaporated *in vacuo*. The residue was re-dissolved in cold dichloromethane and the above step was repeated twice to give a white solid (1.08 g, 90%). ¹H NMR (d₄-THF, ppm): δ 8.97 (s, 1H), 7.93 (d, 2H, ArH), 7.64 (d, 2H, ArH), 1.51 (s, 9H).

P(VDF-PFSVE) with amine end groups. 4,4'-tert-But-oxy-carbonylamino benzoyl peroxide (335 mg, 0.75 mmol), 1,1,1,3,3-pentafluorobutane (15 mL), acetonitrile (15 mL) and a certain amount of PFSVE (see Table 1) were added into a 70 mL Parr reactor with a magnetic stir. The gas-condense transfer of VDF (15 mL) was carried out with the rigorous exclusion of oxygen and moisture through a dual-manifold Schlenk line with 10⁻⁶ Torr high vacuum. The reactor was immersed in an oil bath at 90 °C for 8 h. After residual gases were discharged, the solvents were evaporated, and the residue was dissolved in acetone and precipitated from cold hexane. P(VDF-PFSVE) was collected and dried *in vacuo* at 60 °C. ¹H MMR (d₆-DMSO, ppm): δ 9.67 (s, -NH-), 8.17 (d, ArH), 7.51 (d, ArH), 4.63 (m, -Ph(C=O)O-CH₂CF₂-), 2.9 (-CF₂CH₂-CF₂CH₂-, head-to-tail structure), 2.3 (-CF₂CH₂-CH₂CF₂-, tail-to-tail structure), 1.58 (s, -CH₃).

To a mixture of *tert*-butoxycarbonyl amino terminated P(VDF-PFSVE) (0.5 g) in anhydrous dichloromethane (15 mL) 3 drops of iodotrimethylsilane was added at 0 °C. After being stirred for 3 h, the reaction mixture was condensed under reduced pressure and poured into cold hexane to precipitate the polymer. The collected polymer solid was further purified by re-dissolving

in THF, precipitating from water containing a small amount of NaOH (pH ~ 10). The precipitate was then washed thoroughly with neutral water and dried in *in vacuo* at 60 °C. ¹H MMR (d₆-DMSO, ppm): δ 7.67 (d, ArH), 6.59 (d, ArH), 6.19 (s, -NH₂), 4.63 (m, -COO-CH₂CF₂-), 2.9 (-CF₂CH₂-CF₂CH₂-, head-to-tail), 2.3 (-CF₂CH₂-CH₂CF₂-, tail-to-tail). ¹⁹F NMR (d₆-DMSO, ppm): δ -77.0 to -80.0 (-OCF₂CF(CF₃)OCF₂CF₂SO₂F), -92.4 to -95.8 (-CH₂CF₂CH₂-), -110.2 to -110.8 (-CH₂CF₂-CF₂CF(OR_FSO₂F)), -112.3 (-OCF₂CF₂SO₂F), -114.8 and -116.5 (-CH₂CF₂CF₂CH₂-), -123.2 (-CF₂CF(OR_FSO₂F)), -127.8 (-CF(OR_FSO₂F)-CF₂CH₂-), -145.9 (-OCF₂CF(CF₃)OCF₂CF₂SO₂F).

Membrane preparation

A fine-grinded mixture of amino terminated P(VDF-PFSVE) (0.4 g) and 1,3,5-benzene triisocyanate (12 mg) was heated at 180 °C for 1 h. The cross-linked polymer was then placed between two Teflon sheets and hot-pressed into a ~ 80 μm thick film. To hydrolyze the sulfonyl fluoride groups, the film was immersed in a mixture of triethylamine (5 g), methanol (75 mL) and water (75 mL) at 35 °C for 10 h. After being rinsed by de-ionized (DI) water, the film was immersed in 6 M HCl aqueous solution at 35 °C for 12 h followed by being washed with DI water till neutral.

Characterization

Water uptake and ion-exchange capacity (IEC). The water uptake on mass basis was determined gravimetrically. The membrane in acid form was dried under vacuum at 60 °C for 24 h, and cooled to room temperature in a desiccator before measuring the weight in “dry” state, *W_d*. The membrane was then allowed to equilibrate in water at 30 °C for overnight. After removal of the surface water, the weight in “wet” state, *W_w*, was measured. The water uptake was calculated as the percentage increase from the “dry” to “wet” weight related to *W_d*. The IEC of the membrane was determined by titration of the sulfonic acid groups. Membranes were equilibrated in a large excess of 2 M Na₂SO₄ solution for at least 12 h at room temperature prior to titration. The protons released into solution were titrated with 0.02 M NaOH aqueous solution using phenolphthalein as an indicator.

Proton conductivity measurement. In-plane proton conductivity of the membranes was measured by a four-probe AC impedance method. Impedance data was acquired using Solartron 1260 gain phase analyzer over the frequency range of 1 Hz–100 kHz. Conductivity measurements under fully hydrated conditions were performed after the samples were equilibrated in water at various temperatures for at least 4 h. Temperature was varied from room temperature to 80 °C.

Methanol permeability measurement. The methanol permeability was determined in a standard membrane separated diffusion cell. A glass cell containing solutions A and B in two identical compartments separated by the test membranes was utilized for the permeability tests. The membranes were placed between the two compartments by a screw clamp. Solution A was

a methanol aqueous solution with different concentrations and solution B was DI water. Both compartments were magnetically stirred during the permeation experiments. The concentration of methanol in solution B was evaluated using a differential refractometer. The methanol permeability was calculated from the slope of the straight-line plot of methanol concentration *versus* permeation time. The methanol permeability was tested at temperatures ranging from 30 to 70 °C.

Water state. To characterize the state of absorbed water in the hydrated membranes, low temperature DSC measurements were performed. Fully hydrated membrane samples (10–13 mg) were blotted with a lab wipe to remove surface water, and then instantly placed into a DSC pan (O-ring model TA Instruments) and sealed. The sample was immediately put in the calorimeter and cooled to $-80\text{ }^{\circ}\text{C}$. In a typical run, after being held at $-80\text{ }^{\circ}\text{C}$ for 20 min, the samples were heated to $100\text{ }^{\circ}\text{C}$ at a heating rate of $5\text{ }^{\circ}\text{C min}^{-1}$. The heat of fusion for the water in the membranes was estimated from $\Delta H_f = H/m_{\text{H}_2\text{O}}$, where ΔH_f is the heat of fusion for the water contained in the sample, $m_{\text{H}_2\text{O}}$ is the mass of water within the sample, and H is the integrated energy from the melting endotherm. The ΔH_f value for bulk water is 334 J g^{-1} .

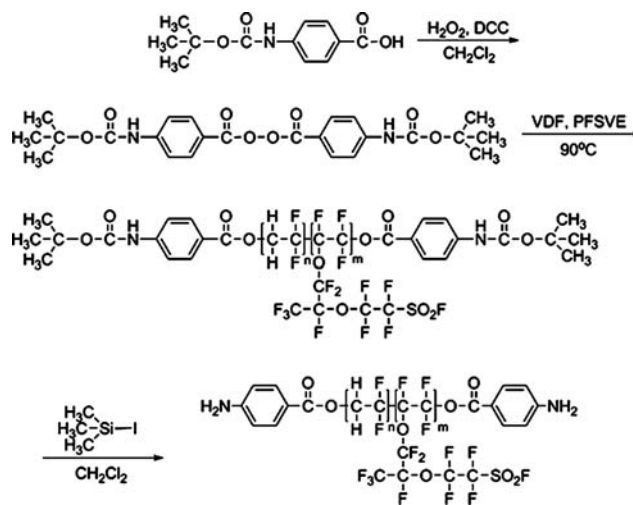
Stability. Oxidative stability of the cross-linked membranes was tested by immersing membrane samples in Fenton's reagent (3% H_2O_2 containing 2 ppm FeSO_4) at $60\text{ }^{\circ}\text{C}$ for 1 h. Hydrolytic stability was estimated by soaking the membrane in DI water at $80\text{ }^{\circ}\text{C}$ for 2 weeks. Before and after the stability testing, all membranes were dried under vacuum at $60\text{ }^{\circ}\text{C}$ overnight and weighed. Gravimetric analyses were conducted after these treatments.

Results and discussion

Synthesis and preparation of the cross-linked membranes

Chain-end functionalization of fluoropolymers is notoriously difficult due to a lack of suitable living/controlled polymerization techniques for fluorinated alkenes. The telomerization process with alkyl halides as transfer agents, is a commonly used method to produce halogen-terminated fluoropolymers, and usually generates low molecular weight ($<4,000\text{ g mol}^{-1}$) fluorinated oligomers.²⁴ More recently, we have developed a new synthetic route toward high molecular weight fluoropolymers with well-defined functional end-groups,^{25,26} in which functionalized benzoyl peroxides (BPOs) are used as the initiator in radical polymerization of fluorinated alkenes. The domination of the radical coupling reaction and absence of disproportionation in the termination process of polymerization allow for the complete transfer of functional groups carried by the initiators into the polymer chain ends upon polymerization.²⁷

As illustrated in Scheme 1, BPO containing *t*-butoxycarbonyl (Boc) protected amine groups was synthesized from the homocoupling of Boc-amino-benzoic acid in the presence of H_2O_2 and *N,N'*-dicyclohexylcarbodiimide (DCC). The functional BPO was subsequently utilized as the initiator for co-polymerization of VDF and PFSVE. The polymerization was carried out in the presence of 0.5 mol% of the functional initiator, and a mixture solvent of acetonitrile and 1,1,1,3,3-pentafluorobutane that has



Scheme 1 Scheme showing the synthesis of amino-terminated P(VDF-PFSVE).

minimized chain transfer reactions. The presence of the Boc moieties at polymer chain ends were confirmed by the $^1\text{H NMR}$ spectra. As shown in Fig. 1a, the signals at 1.58, 8.17 and 7.51 ppm are assigned to the protons of *tert*-butyl and phenyl groups, respectively. Amine groups were released from Boc protecting groups using iodotrimethylsilane, as evidenced by disappearance of the peak at 1.58 ppm belonging to *tert*-butyl groups and emergence of resonances at 6.19 ppm attributed to amine groups as shown in Fig. 1b. The small triplet in the region of 6.2–6.6 ppm corresponds to a $-\text{CF}_2\text{H}$ group resulting from a short chain-branching process, which involves an intramolecular 1–5 hydrogen shift analogous to similar radical reactions reported in low-density polyethylene.

As summarized in Table 1, by manipulating the monomer feed ratio and the reaction time, P(VDF-PFSVE) copolymers (I–IV)

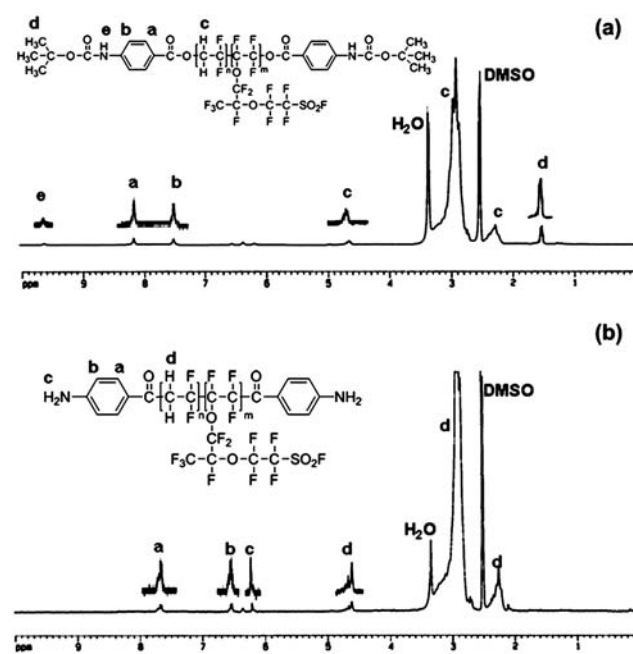


Fig. 1 $^1\text{H NMR}$ spectra of chain-end functionalized P(VDF-PFSVE)s.

Table 1 Chemical composition and molecular weight characteristics of P(VDF-PFSVE) copolymer

Copolymer	Monomer ratio (mol%)		Composition (mol%)		$M_{n, GPC}/g\ mol^{-1}$	PDI
	VDF	PFSVE	VDF	PFSVE		
I	94	6	94.7	5.3	19,800	1.6
II	91	9	91.5	8.5	20,600	1.6
III	88	12	89.8	10.2	17,400	1.6
IV	85	15	86.9	13.1	16,600	1.7

with the PFSVE content ranging from 5.3 to 13.1 mol% were obtained. The copolymer compositions were determined using 1H and ^{19}F NMR spectroscopy.²⁸ The number-average molecular weights of the polymers were around 16–20 kg mol⁻¹ with polydispersities of ~1.7.

The cross-linking of P(VDF-PFSVE)s was conducted through a condensation reaction between amine end-groups and a triisocyanate agent. FTIR spectra confirmed the formation of urea linkages by the appearance of urea bands at 3348 cm⁻¹ (N–H stretching vibration), 1632 cm⁻¹ (C–N stretching), and 1546 cm⁻¹ (N–H bending) and a lack of absorbance at 2267 cm⁻¹ from isocyanate groups. The accomplishment of cross-linking was also supported by the changes of solubility in organic solvents. The cross-linked membranes became insoluble in acetone, tetrahydrofuran and methanol, whereas their precursors, P(VDF-PFSVE)s, can be easily dissolved in these solvents. A further evidence for the cross-linking reaction was provided by thermal analysis. The cross-linked membrane showed a broader melting transition at ~120 °C, and the crystallization temperature was found to decrease by nearly 7 °C relative to its polymer precursor (~79 °C). It is known that the formation of cross-linking structures suppresses the recrystallization and leads to a reduction in crystal sizes and in turn a lower crystallization temperature.²⁵

Hydrolysis of the sulfonyl fluoride groups in the membranes is required to generate the proton conducting acid sites. Strong bases such as sodium hydroxide and potassium hydroxide are usually used in the hydrolysis of sulfonyl fluorides. However, they are undesirable here because of the vulnerability of VDF units under basic conditions.²⁹ Lithium carbonate has been employed as a mild catalyst for base hydrolysis³⁰ but unfortunately, the lack of solubility in protic solvents that are used in swelling the cross-linked films limits its utility in this case. To this end, a new mild hydrolysis process was developed, which is based on triethylamine/methanol as a catalyst to convert sulfonyl fluoride groups into ammonium salts.³¹ Ion exchange was accomplished with HCl aqueous solution, which was confirmed by the complete disappearance of S–F stretching resonance at 816 cm⁻¹ in the FTIR spectra. Concurrently, the FTIR spectra of the sulfonic acid form of the films showed the characteristic absorbance of -SO₂F groups at 1462 cm⁻¹ attributed to S = O stretching and a broad peak assigned to acid groups at 3000 to 3300 cm⁻¹. The retention of the urea linkages in the acid membranes was indicated by the unchanged absorption band at 1632 cm⁻¹.

IEC and water uptake

Table 2 compares the characteristics of the cross-linked membranes. The IEC of the membranes increases with the

Table 2 The IEC, water uptake, hydration number (λ) and heat of fusion (ΔH_f) of absorbed water of the cross-linked P(VDF-PFSVE) membranes and Nafion 117

Membrane	IEC (meq/g)		Water Uptake (wt.%)	λ	$\Delta H_f/J\ g^{-1}$
	IEC ^a	IEC ^b			
I	0.63	0.45	4	4.9	10
II	0.89	0.87	14	8.9	24
III	0.99	0.97	19	10.6	61
IV	1.15	1.14	26	12.6	98
Nafion 117		0.91	29	17.7	101

^a Calculated from copolymer compositions. ^b Determined by titration method.

increase of PFSVE content. In membranes **II**, **III** and **IV**, experimental IEC results were found to be in good agreement with their corresponding theoretical values estimated from VDF/PFSVE composition. This further indicates the quantitative conversion of salt into acid forms of the films and the effectiveness of the new hydrolysis procedure. The deviation shown in membrane **I** is believed to be owing to low sulfonate content and difficulty in formation of a continuous ionic phase that is accessible for ion exchange.

As expected, higher IEC membranes have increased water uptake as a result of increased amount of acid groups interacting with water molecules. Interestingly, in comparison with Nafion 117 film that has an IEC of 0.91 mmol g⁻¹ and a water uptake of 29%, membranes **II** and **III** with similar IEC values of 0.87 and 0.97 mmol g⁻¹ exhibited much lower water uptakes, only 14% and 19% respectively. Additionally, it is worthy of note that negligible change of water uptake was observed in the cross-linked membranes when temperature was increased to 60 °C, which is indicative of stabilized water domain structures by the cross-linked networks. Analogous to water uptake, hydration number λ , *i.e.* the average number of water molecules per sulfonic acid group, showed strong dependence on IEC as well. As outlined in Table 2, when IEC was increased to or more than 0.87 mmol g⁻¹, λ attained a value of 8.9 or higher, which suggests sufficiently high hydration levels in the membranes to facilitate dissociation of sulfonic acid and proton transportation.

Thermal and chemical stability

Thermal stability was evaluated by thermal-gravimetric analysis. As shown in Table 3, the on-set decomposition temperatures of the cross-linked membranes were independent of IEC and stayed in the narrow range 265–270 °C, which is comparable with Nafion. Accelerated hydrolytic and oxidative stability tests combined with gravimetric and tensile measurements were also executed to assess the chemical stability of the membranes. It was found that the cross-linked membranes remained intact and retained more than 95% of their original weight and modulus after the tests, indicating their excellent hydrolytic and oxidative stabilities. We postulate that the urea linkages, the most susceptible segment to hydrophilic attack by water molecules and oxidative attack by radical species, is protected by the surrounding hydrophobic fluorinate chains that exclude water molecules and OH radicals in aqueous solution.

Table 3 Thermal, hydrolytic and oxidative stability of the cross-linked P(VDF-PFSVE) membranes and Nafion 117

Membrane	$T_d/^\circ\text{C}$	Residue after hydrolytic testing (wt.%)	Residue after oxidative testing (wt.%)
I	270	98	98
II	265	97	98
III	267	97	98
IV	265	95	96
Nafion 117	275	99	98

Membrane morphology

Morphological structures in the cross-linked membranes and Nafion were examined by TEM. Fig. 2 presents cross-sectional TEM images of the membranes stained with lead acetate, in which ionic domains appear as dark areas due to their affinity with lead ions and the bright domains correspond to the hydrophobic phases. It was found that the sizes of the ionic aggregates in the cross-linked membranes displayed gradual increases from **I** to **IV** due to the increased sulfonic acid concentrations. A microphase-separated morphology with hydrophilic domain size at the scale of 5–10 nm was evident in Nafion. Contrastingly, phase separation in the cross-linked membranes (Fig. 2b–e) was not as distinct as in Nafion. The size of the ionic regions in the cross-linked membranes is markedly smaller than that of Nafion, *e.g.* an average of only 2–3 nm in membranes **III** and **IV** with IECs even higher than Nafion. It appears that self-assembly behaviors in these membranes are hindered by the formation of cross-linked structure, leading to small ionic aggregates and in turn limited water absorption.

The state of absorbed water

In addition to membrane morphology, the state of the absorbed water within the membranes has also been suggested to play

a significant role in determining the transport properties.^{32,33} It is speculated that the permeation of methanol through ionic membranes is strongly correlated to the unbound or free water.³⁴ Free water is defined as water that is not intimately bound to polymer backbone or ionic groups and exhibits similar thermal transitions to bulk water. The low temperature DSC measurements were carried out to elucidate the nature of water confined in the membranes. Fig. 3 illustrates DSC curves of the fully hydrated membranes, and the calculated ΔH_f of the absorbed water is tabulated in Table 2. Since the strongly bound water does not display thermal transitions and contribute to the melting endotherm, the ΔH_f value is generally proportional to the fraction of free and weakly bound water. Consistent with the trend in λ and water uptake, ΔH_f has been found to increase simultaneously with increasing IEC. Membranes **I** and **II** contained primarily bound water as indicated by indiscernible melting endotherms and low ΔH_f values, 10 and 24 J g⁻¹ respectively. Membranes **III** and **IV** showed higher ΔH_f values of 61 and 98 J g⁻¹ respectively, indicating an increased fraction of unbound and weakly bound water, but still less than Nafion with a ΔH_f of 101 J g⁻¹.

Proton conductivity and methanol permeability

Fig. 4a depicts the effect of IEC on the proton conductivity and activation energy. In accordance with water uptake and λ , the proton conductivity rose progressively from 0.005 S cm⁻¹ for membrane **I** to 0.063 S cm⁻¹ for membrane **IV** with the increase of IEC. In comparison with Nafion, the cross-linked membranes exhibited reduced proton conductivities. The difference in conductivity between Nafion and the cross-linked membranes is probably due to the concomitant higher content of water sorption and corresponding enhancement of phase separation in Nafion. It is important to note that membranes **II**, **III** and **IV** exhibited appreciably high conductivities of above 0.02 S cm⁻¹, attributable to their high concentrations of PFSVE and strong acidity of perfluorosulfonic acid groups. Activation energy for

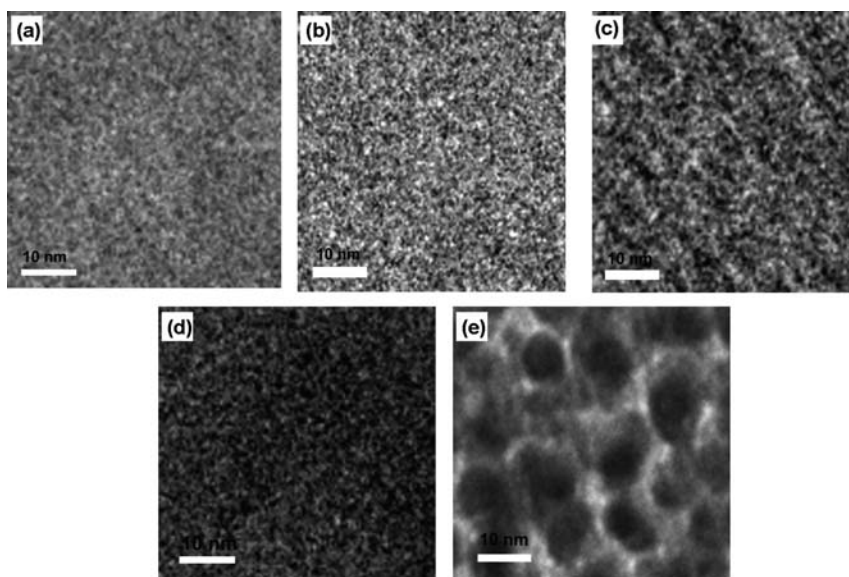


Fig. 2 Cross-sectional TEM images of (a) Nafion 117 and the cross-linked membranes, (b) I, (c) II, (d) III and (e) IV. The scale bar denotes 10 nm.

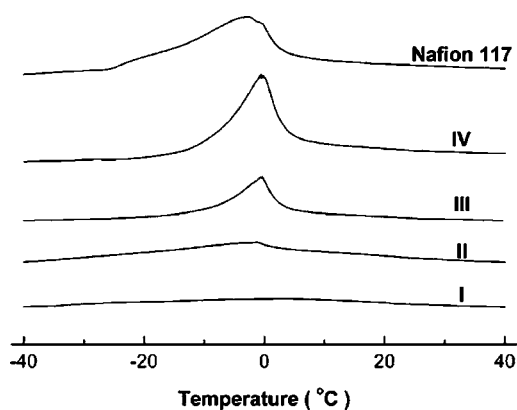


Fig. 3 DSC curves of the melting endotherms for the absorbed water within the cross-linked membranes and Nafion 117.

proton conduction, $E_{a,\sigma}$, is a measure of the barrier to proton movement occurring in the membrane. $E_{a,\sigma}$ was calculated from the Arrhenius plot, where the proton conductivity of the membranes was measured in liquid water at various

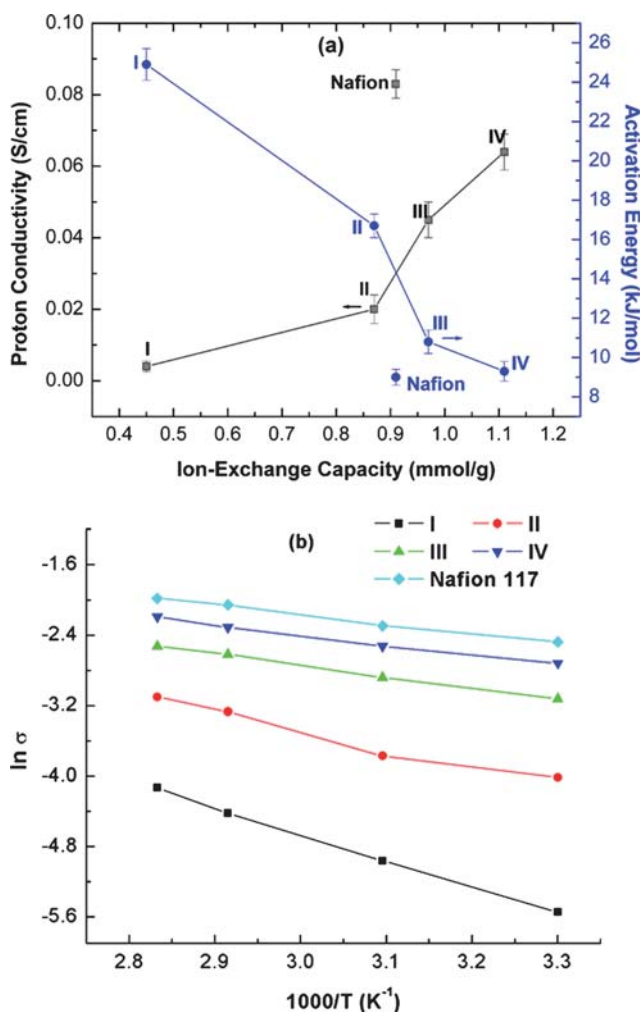


Fig. 4 (a) Proton conductivity and activation energy of the cross-linked membranes as a function of IEC at 30 °C. (b) Temperature dependence of proton conductivity of the membranes under fully hydrated conditions.

temperatures (Fig. 4b). The highest value of $E_{a,\sigma}$ was found with membrane I followed by membranes II, III and then IV. Nafion exhibited the lowest value of $E_{a,\sigma}$. This order mirrors that of proton conductivity and correlates well with the amount of water contained in the membrane and the domain sizes of hydrophilic phases.

Methanol permeability and related activation energy data are plotted as a function of IEC in Fig. 5a. Extremely low methanol permeabilities of 1.12×10^{-9} and $8.36 \times 10^{-9} \text{ cm}^2 \text{ s}^{-1}$ were found with membranes I and II respectively, which are more than two orders of magnitude less than Nafion with a methanol permeability of $1.96 \times 10^{-6} \text{ cm}^2 \text{ s}^{-1}$. The high fraction of strongly bound water as revealed in low ΔH_f values from DSC measurements and small size of ionic domains are likely responsible for the observed excellent methanol barrier properties in the membranes. Further increase in IEC leads to a monotonic increase in methanol permeability. Membranes III and IV exhibit methanol permeabilities of 4.98×10^{-8} and $1.35 \times 10^{-6} \text{ cm}^2 \text{ s}^{-1}$, respectively, which are still much lower than Nafion. The activation energy for methanol permeation, $E_{a,\text{methanol}}$, estimated from the Arrhenius plot of methanol permeability

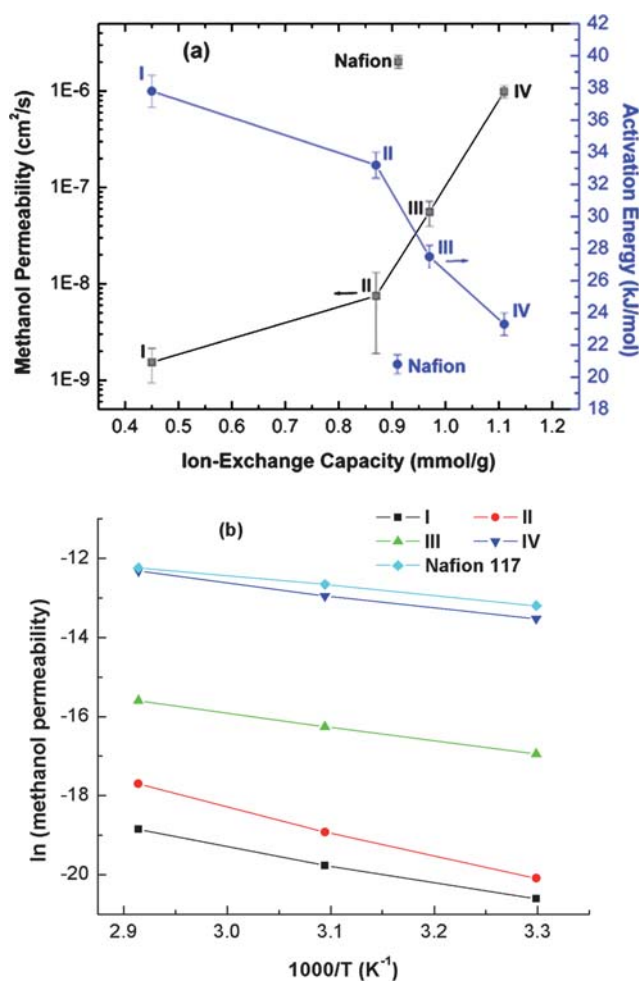


Fig. 5 (a) Methanol permeability and activation energy of the cross-linked membranes as a function of IEC at 30 °C. (b) Temperature dependence of methanol permeability of the membranes under fully hydrated conditions.

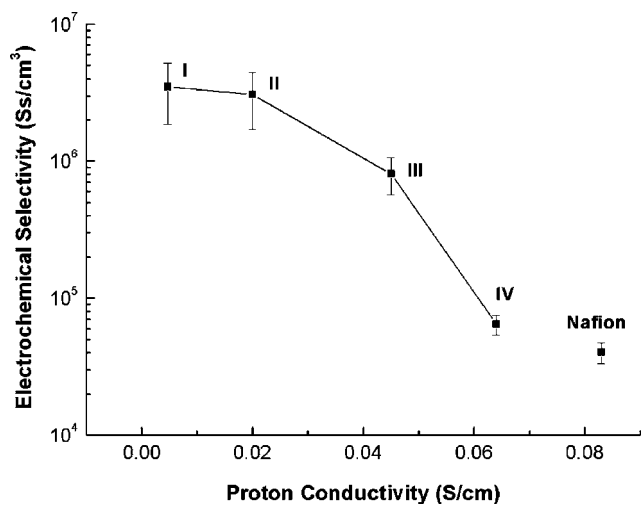


Fig. 6 Electrochemical selectivity of the cross-linked membranes and Nafion 117.

(Fig. 5b), follows the same trend with $E_{a,\sigma}$. Higher values of $E_{a,\text{methanol}}$ reiterate elevated barriers to methanol transport in the cross-linked membranes when compared to Nafion. Considerable changes in methanol permeability upon IEC is presumably associated with significant variation in the water state and domain structure. Expanded ionic channels and the increased portion of unbound and weakly bound water give rise to greater methanol diffusion across the membrane.

To evaluate the potential of the prepared membranes for DMFCs, the electrochemical selectivity is computed and plotted versus IEC as shown in Fig. 6. Encouragingly, the cross-linked membranes have shown very high selectivity in transport of protons over methanol. The reduced methanol permeability significantly outweighs the decrease in ionic conductivity in the cross-linked membranes. More impressively, the electrochemical selectivities of the membranes **II** and **III** are 1.2×10^7 and 9.2×10^5 , respectively, which are 288 and 22 times respectively higher than that of Nafion (*i.e.* 4.2×10^4) while maintaining high proton conductivities ($> 0.02 \text{ S cm}^{-1}$). To the best of our knowledge, this is the highest electrochemical selectivity reported from PEMs with proton conductivities higher than 0.01 S cm^{-1} .⁷ The exceptional selectivity obtained in the cross-linked membranes may be attributed to the unique interplay of a high fraction of strongly-bound water, small-sized transport channels, and the superior acidity of perfluorosulfonic acid groups.

Conclusions

A series of P(VDF-PFSVE) with amino end-groups and varied contents of perfluorosulfonic acids have been prepared and fabricated into cross-linked membranes after curing with a triisocyanate agent. The formation of cross-linked structures restricts the size of the hydrophilic domains, limits water sorption and yields a high content of tightly bound absorbed water. Membrane properties including water uptake, the state of absorbed water and morphological structure have been found to be strongly related to IEC. Sharp growth in the fraction of loosely bound and unbound water and the size of the ionic

domains has been observed with increasing IEC, which in turn leads to significant variation in transport properties. Membranes with relatively low IECs exhibit extremely low methanol permeability, which are ascribed to a large portion of tightly bound water and small sized ionic aggregates. Membranes **II** and **III** exhibit unparalleled electrochemical selectivities that are two orders of magnitude higher than Nafion, while maintaining sufficient proton conductivity (*i.e.* $> 0.02 \text{ S m}^{-1}$). The lower methanol crossover of the cross-linked membranes has also been demonstrated in the preliminary membrane-electrode assembly (MEA) studies. The open circuit voltages of membranes **II** and **III** under 3 M methanol/air conditions at 50°C were found in a range of 0.75 to 0.85 V, which is much greater than that of Nafion 117 ($\sim 0.65 \text{ V}$).

Acknowledgements

This work was supported by the National Science Foundation (CBET-0932740).

References

- 1 F. Barbir, *PEM Fuel Cells: Theory and Practice*, Academic Press, New York, 2005.
- 2 B. Gurau and E. S. Smotkin, *J. Power Sources*, 2002, **112**, 339.
- 3 A. Heinzel and V. M. Barragan, *J. Power Sources*, 1999, **84**, 70.
- 4 A. A. Kulikovskiy, *J. Electrochem. Soc.*, 2005, **152**, A1121.
- 5 S. Kang, S. J. Lee and H. Chang, *J. Electrochem. Soc.*, 2007, **154**, B1179.
- 6 J. T. Wang, S. Wasmus and R. F. Savinell, *J. Electrochem. Soc.*, 1996, **143**, 1233.
- 7 N. W. Deluca and Y. A. Elabd, *J. Polym. Sci., Part B: Polym. Phys.*, 2006, **44**, 2201.
- 8 R. Dillon, S. Srinivasan, A. S. Arico and V. Antonucci, *J. Power Sources*, 2004, **127**, 112.
- 9 M. Sankir, Y. S. Kim, B. S. Pivovar and J. E. McGrath, *J. Membr. Sci.*, 2007, **299**, 8.
- 10 V. S. Silva, B. Ruffmann, S. Vetter, M. Boaventura, A. M. Mendes, L. M. Madeira and S. P. Nunes, *Electrochim. Acta*, 2006, **51**, 3699.
- 11 K. Xu, C. Chanthad, M. R. Gadinski, M. A. Hickner and Q. Wang, *ACS Appl. Mater. Interfaces*, 2009, **1**, 2573.
- 12 D. J. Jones and J. Roziere, *Adv. Res. Polym. Sci.*, 2008, **215**, 219.
- 13 G. Alberti and M. Casciola, *Annu. Rev. Mater. Res.*, 2003, **33**, 129.
- 14 J. A. Kerres, *Fuel Cells*, 2005, **5**, 230.
- 15 C. W. Lin, Y. F. Huang and A. M. Kannan, *J. Power Sources*, 2007, **171**, 340.
- 16 R. Wycisk, J. Chisholm, J. Lee, J. Lin and P. N. Pintauro, *J. Power Sources*, 2006, **163**, 9.
- 17 J. Wootthikanokkhan and N. Seeponkai, *J. Appl. Polym. Sci.*, 2006, **102**, 5941.
- 18 N. W. DeLuca and Y. A. Elabd, *J. Power Sources*, 2006, **163**, 386.
- 19 K. Miyatake, H. Zhou and M. Watanabe, *Macromolecules*, 2004, **37**, 4956.
- 20 M. Rikukawa and K. Sanui, *J. Membr. Sci.*, 2004, **233**, 93.
- 21 B. Bae, H. Y. Ha and D. Kim, *J. Membr. Sci.*, 2006, **276**, 51.
- 22 L. Sauguet, B. Ameduri and B. Boutevin, *J. Polym. Sci., Part A: Polym. Chem.*, 2006, **44**, 4566.
- 23 S. J. Atkinson, V. E. Ellis, S. E. Boyd and C. L. Brown, *New J. Chem.*, 2007, **31**, 155.
- 24 B. Boutevin, *J. Polym. Sci., Part A: Polym. Chem.*, 2000, **38**, 3235.
- 25 K. Li, S. Liang, Y. Lu and Q. Wang, *Macromolecules*, 2007, **40**, 4121.
- 26 K. Xu, K. Li, P. Khanchaitit and Q. Wang, *Chem. Mater.*, 2007, **19**, 5937.
- 27 J. Guiot, B. Ameduri and B. Boutevin, *Macromolecules*, 2002, **35**, 8694.
- 28 K. Xu, K. Li, C. S. Ewing, M. A. Hickner and Q. Wang, *Macromolecules*, 2010, **43**, 1692.

-
- 29 D. A. Seiler, *Modern Fluoropolymers*, Wiley, New York, 1997, pp. 487.
- 30 Z. Y. Yang, L. Wang, N. E. Drysdale and M. Doyle, *Macromolecules*, 2003, **36**, 8205.
- 31 Y. Li, Z. Q. Chen, J. Tian, Y. B. Zhou and Z. X. Chen, *J. Fluorine Chem.*, 2004, **125**, 1077.
- 32 M. A. Hickner, C. H. Fujimoto and C. J. Cornelius, *Polymer*, 2006, **47**, 4238.
- 33 Y. S. Kim, M. A. Hickner, L. Dong, B. S. Pivovar and J. E. McGrath, *J. Membr. Sci.*, 2004, **243**, 317.
- 34 A. Siu, B. Pivovar, J. Horsfall, K. V. Lovell and S. Holdercroft, *J. Polym. Sci., Part B: Polym. Phys.*, 2006, **44**, 2240.